Finding Membrane Shells Subjected to Horizontal Body Forces with Radial Basis Functions

Chiang, Y.-C.; Borgart, Andrew; Li, Qingpeng

Important note
To cite this publication, please use the final published version (if applicable).
Please check the document version above.

Finding Membrane Shells Subjected to Horizontal Body Forces with Radial Basis Functions

Yu-Chou CHIANG*, Andrew BORGART, Qingpeng LI[a]

* Faculty of Architecture and Built Environment, Delft University of Technology
Chiang.YuChou@gmail.com

[a] School of Architecture and Urban Planning, Nanjing University

Abstract

Membrane shells, which have minimized bending moments under certain load conditions, are regarded as ideal structural forms in terms of material efficiency. Most of the existing numerical form-finding methods are based on discretizing membranes into finite panels or funicular networks and focusing on gravitational loading only. In order to obtain smooth shells and to consider horizontal loads, this paper presents a method to find the equilibrium forms of the membrane shells by solving Pucher's equation. Radial base functions (RBFs) is utilized to represent stresses and shapes of the membranes, and a least square method is applied to find the controlling coefficients which allow the functions to fit the boundary conditions (e.g. zero stresses at the free edges) and the governing equation. When all the parameters are carefully chosen, the stress and shape functions can achieve sufficient accuracy. The presented method has been preliminarily implemented to find shells on a triangle ground plan incorporating horizontal loads. The form-found geometries are then analyzed by finite element models. The result confirms that the form-found shells have the stress distributions similar to the prescribed stresses.

Keywords: from finding, membrane shells, radial basis functions, Pucher's equation, funicular structures.

1. Introduction

The design of membrane shells is to contain stresses in the curved surface (force follows form) and to curve the surface following the embedded stresses (form follows forces). By carefully designing the stresses and the surfaces, membrane shell structures can elegantly span large area with minimal materials by membrane stresses (i.e. tension, compression, and in-plane shear stresses).

Although the shells are materially efficient structures, the complication of the shell theory prohibits them to be widely applied [1] (let alone the fabrication of the doubly curved surfaces). By the development of computational methods and techniques, numerical algorithms are able to analyze the statics of the shells by discretizing the continuous surfaces into finite elements [2] and sometimes reconstruct them back to smooth NURBS surfaces [3]. However, the design of smooth shells is still restricted to a few analytical solutions.

The aim of this paper is to utilize radial basis functions (RBFs), a numerical method developed in the 1990s, which can easily represent free-form C^∞ smooth multivariate functions and facilitate scientists solving partial differential equations (PDEs)[4], [5]. Surprisingly, the method has not been applied for form-finding application, to the best of authors' knowledge. This paper investigates how to apply RBFs to represent both stress and shape functions and how to find an agreement between them by solving Pucher's equation. The investigation shows the RBFs are handy numerical design tools to even handle horizontal body forces and the singularity of the point-supported membrane shells.

The outline of this paper is as follow. The first section introduces the features of membrane shells. The second section briefly explains how to apply RBFs to represent an arbitrary function and its differential operation. The third section focuses on the Pucher's equation and related boundary conditions. The fourth section proposes an overall workflow with a demonstration finding shapes of membrane shells on a triangular ground plane. The fifth section concludes the current finding and projects future works.

2. Basic Operations of Radial Basis Functions

Radial basis functions are used to represent a smooth multivariate function. An arbitrary function $f(\mathbf{x})$ can be approximated by a serious of radial basis functions $\phi(\|\mathbf{x} - \mathbf{\mu}_i\|; \rho_i)$ and polynomial terms $h(\mathbf{x})$ [4]:

$$f(\mathbf{x}) = \sum_{i=1}^{n} \lambda_i \phi(\|\mathbf{x} - \mathbf{\mu}_i\|; \rho_i) + h(\mathbf{x}) + \varepsilon , \qquad (1)$$

in which $\mathbf{x}$ is the position of evaluation, λ_i are the magnitude coefficients of the RBFs, $\mathbf{\mu}_i$ are the source points, ρ_i are the shape parameter of the RBFs, and ε is the approximate error. By sufficient number of RBFs n, the equation (1) shall be able to deliver decent accuracy.

For a linear differential operator $\mathcal{D}[\cdot]$ acting on the function $f(\mathbf{x})$, the derivative equation would be

$$\mathcal{D}[f(\mathbf{x})] = \sum_{i=1}^{n} \lambda_i \cdot \mathcal{D}\left[\phi(\|\mathbf{x} - \mathbf{\mu}_i\|; \rho_i)\right] + \mathcal{D}[h(\mathbf{x})] + \varepsilon_{\mathcal{D}} . \qquad (2)$$

which also can be presented in a matrix form:

$$\mathcal{D}[\mathbf{f}(\mathbf{x})] = \begin{bmatrix} \mathcal{D}[\mathbf{\Phi}(\mathbf{x})] & \mathcal{D}[\mathbf{H}(\mathbf{x})] \end{bmatrix} \begin{bmatrix} \mathbf{\lambda} \\ \mathbf{c} \end{bmatrix} + \mathbf{\varepsilon}_{\mathcal{D}} , \qquad (2a)$$

in which $\mathbf{\lambda}$ are the magnitude coefficients of the radial basis functions, while $\mathbf{c}$ are the coefficients of the polynomial terms. The coefficients then can be regarded as the main arguments for minimizing the squared approximate errors. When the desired derivative values of the function ($\mathbf{g}_{xa}$) are provided at certain locations ($\mathbf{x}_a$), coefficient vectors can be provided by the weighted least square method:

$$\begin{bmatrix} \mathbf{\lambda} \\ \mathbf{c} \end{bmatrix} = \left(\mathbf{A}^T \mathbf{W} \mathbf{A}\right)^{-1} \mathbf{A}^T \mathbf{W} \mathbf{g}_{xa} \qquad (3)$$

where $\mathbf{A}$ is defined by $\begin{bmatrix} \mathcal{D}[\mathbf{\Phi}(\mathbf{x})]\big|_{\mathbf{x}=\mathbf{x}_a} & \mathcal{D}[\mathbf{H}(\mathbf{x})]\big|_{\mathbf{x}=\mathbf{x}_a} \end{bmatrix}$, and $\mathbf{W}$ is the weight matrix.

Having the basic differential and the least-square operations of the RBFs in mind, the following sections state the specific differential operations should be concerned for designing a membrane shell.

3. Pucher's Equation and Boundary Conditions

The overall aim of designing membrane shells is to determine the equilibrium state of the membrane surface. Fortunately, the Airy stress function can describe the internal equilibrium of the 2D stress fields succinctly with a scalar function, and the C^0 continuation of the stress function guarantees the equilibrium in the two directions. The equilibrium stresses can be expressed as follow when body forces are also considered [6]:

$$\begin{aligned} \bar{N}_{11} &= \partial_{22}F - \int \bar{p}_1 dx_1, \\ \bar{N}_{12} &= -\partial_{12}F, \\ \bar{N}_{22} &= \partial_{11}F - \int \bar{p}_2 dx_2, \end{aligned} \qquad (4)$$

in which $\bar{N}_{11}$ and $\bar{N}_{22}$ are normal stress in two directions, $\bar{N}_{12}$ is the in-plane shear stress, F is the Airy stress function, $\bar{p}_1$ and $\bar{p}_2$ are the body forces per unit area in related directions. ∂_{12} is the Euler's

notation for the mixed second partial derivative, meanwhile ∂_{11} and ∂_{22} are the derivatives with respect to the coordination 1 and 2.

While the Airy stress function guarantees the horizontal equilibrium, the equilibrium in z-direction is governed by the Pucher's equation [6]:

$$\bar{N}_{11} \cdot \partial_{11}z + 2\bar{N}_{12} \cdot \partial_{12}z + \bar{N}_{22} \cdot \partial_{22}z = \bar{p}_1 \cdot \partial_1 z + \bar{p}_2 \cdot \partial_2 z - \bar{p}_z . \tag{5}$$

When the external loads $\bar{p}_1$, $\bar{p}_2$, and $\bar{p}_z$ are given, the designer only needs to find a set of the stress function $F(\mathbf{x})$ and shape function $z(\mathbf{x})$ that meet both of the equations (4) and (5).

Within the Pucher's equation, either the shape function $z(\mathbf{x})$ or the stress function $F(\mathbf{x})$ can be regarded as unknown, and others are assumed independent of the unknown functions. Explicitly, when the loads and the stresses are given, the shape function should be governed by

$$[(\partial_{22}F - \int \bar{p}_1 dx_1) \cdot \partial_{11} - 2\partial_{12}F \cdot \partial_{12} + (\partial_{11}F - \int \bar{p}_2 dx_2) \cdot \partial_{22} - \bar{p}_1 \cdot \partial_1 - \bar{p}_2 \cdot \partial_2]z = -\bar{p}_z , \tag{5a}$$

or in an abridged notation as $\mathcal{P}_z^{\mathcal{F}}[z] = -\bar{p}_z$, where $\mathcal{P}_z^{\mathcal{F}}[\cdot]$ is the differential operator acting on the shape function. In another way around, when the loads and the shape are given, the stress function should meets

$$[\partial_{11}z \cdot \partial_{22} - 2\partial_{12}z \cdot \partial_{12} + \partial_{22}z \cdot \partial_{11}]F = \int \bar{p}_1 dx_1 \cdot \partial_{11}z + \int \bar{p}_2 dx_2 \cdot \partial_{22}z + \bar{p}_1 \cdot \partial_1 z + \bar{p}_2 \cdot \partial_2 z - \bar{p}_z , \tag{5b}$$

or in an abridged notation $\mathcal{P}_F^{\mathcal{Z}}[F] = -\bar{p}_z'$, where $\mathcal{P}_F^{\mathcal{Z}}[\cdot]$ is the differential operator action on the stress function while $-\bar{p}_z'$ is the summation of all the terms on the right-hand side.

Given the fact that the solution of the Airy stress function does not exist in the case of free-edges point-supported parabola membrane shell [1], it might also be possible that an arbitrarily given set of boundary conditions and stress function could not permit the existence of a shape function. In other words, the shape function and stress function should recursively be revised until they mutually agree.

3.2. Boundary Conditions of Stress Functions Subsections

The equilibriums in three directions within the domain are governed by equations (4) and (5). However, the stresses around the boundaries require extra attention. Stresses at the fully supported edges would have no constraints, given that all resultant forces that shell imposes can be balanced by resistance from the supports. In contrast, for free edges, there should have no normal stress transmitting from or towards the boundaries, have no shear stresses against the tangential direction, and have no unbalanced vertical loads. For other common boundary types and their constraints are listed in Table 1. The normal and tangential directions are shown in Figure 1.

In this paper, free-edge is the mainly considered boundary type. The related boundary conditions are

$$\bar{N}_{nn} = 0,$$
$$\bar{N}_{nt} = 0. \tag{6}$$

Table 1 The boundary constraints on the functions.

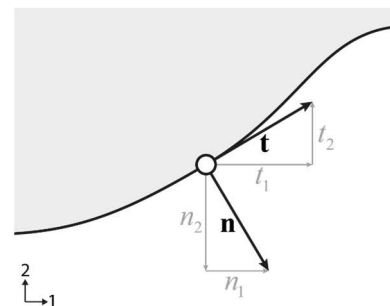| Boundary types	Constraints on functions	
	$\bar{N}$	$\bar{p}_z$
Support	no constraint	no constraint
On diaphragm	$\bar{N}_{nn} = 0$	no constraint
On columns	$\bar{N}_{nn} = 0$, $\bar{N}_{nt} = 0$	no constraint
Reinforced edge	$\bar{N}_{nn} = 0$	$\bar{p}_z = $ self-weight
Free edge	$\bar{N}_{nn} = 0$, $\bar{N}_{nt} = 0$	$\bar{p}_z = $ self-weight

Figure 1 Directions at edges

When the normal vectors and the tangent vectors of the edges are expressed as $\begin{bmatrix} n_1 & n_2 \end{bmatrix}$ and $\begin{bmatrix} t_1 & t_2 \end{bmatrix} = \begin{bmatrix} -n_2 & n_1 \end{bmatrix}$, and equation (4) is incorporated, the conditions of the equation (6) become

$$\partial_{tt}F = n_1^2 \int \overline{p}_1 dx_1 + n_2^2 \int \overline{p}_2 dx_2,$$
$$-\partial_{nt}F = -n_1 n_2 \int \overline{p}_1 dx_1 + n_1 n_2 \int \overline{p}_2 dx_2. \tag{7}$$

The final remark on the conditions of stress function is that only the second derivative, or curvature, of the stress function influence the Pucher's equation. In other words, the stress function can be homogenously elevated or sheered, and the stress field remains the same. Therefore, there are 3 degrees of freedom in the stress function, which regard the overall elevation and overall slops in two directions, shall be constrained in order to acquire a determined solution.

3.3. Boundary Condition of Shape Function

Designers may wish the shell be supported by few given locations. In mathematical terms, it means imposing the Dirichlet boundary condition in the shape function, which can be express as:

$$z(\mathbf{x}_s) = z_s, \tag{8}$$

where $\mathbf{x}_s$ are the location of the supports and z_s are the desired elevations of them.

4. Methodology and Application

Pucher's equation governs the equilibrium of the membrane shell, but it disregards compatibility conditions nor constitutive relation. These features make it a problem with non-unique solutions providing many degrees of freedom for structure designers.

To locate the converged solutions of the stress function and the shape function under the given loads in the Pucher's equation, this paper proposes a workflow of designing a membrane shell as follows:

1. Determine the ground plane. List the boundary conditions of the shell (supports, free edges).
2. Identify potential singular points and arrange the basis functions accordingly.
3a. Design initial shape.   3b. Design initial stress field.
4a. Find the corresponding stress function with the Pucher's equation.   4b. Find corresponding shape function with the Pucher's equation.
5. Revise stress function according to the shape, and revise shape according to the updated stress until two of them converged.

To explicitly show how to precede the design sequence, the sub-sections start with brief explanations that what type of RBF is chosen and the arrangement of them, and followed the implementation of RBFs to find the membrane shells.

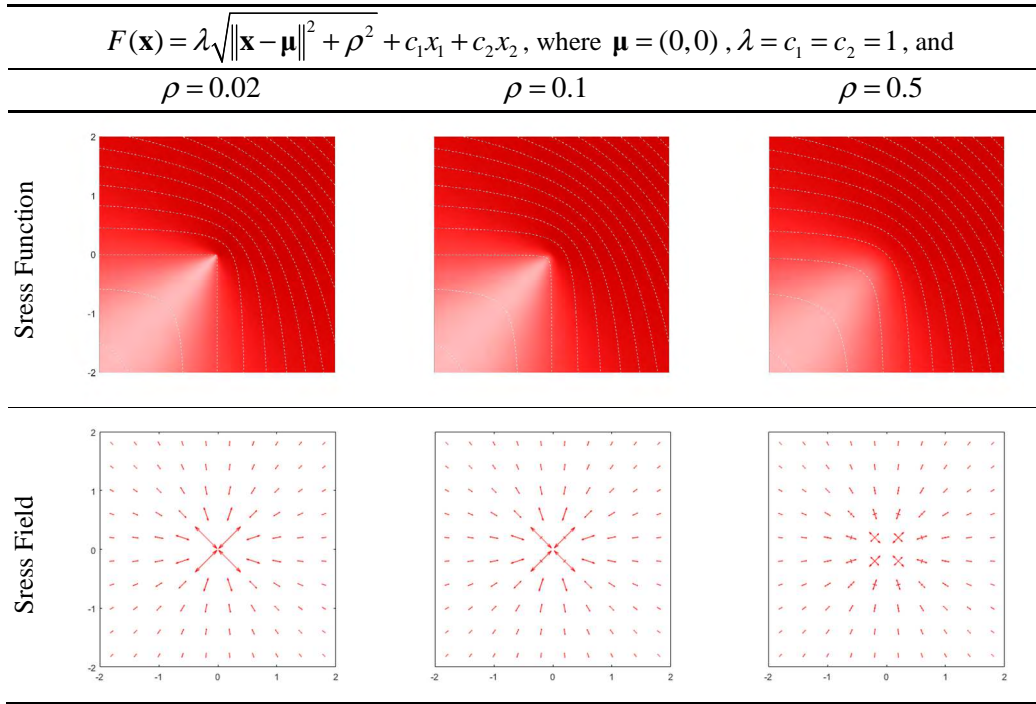### 4.1 Designing the ground-plane and arranging the source and calibration points for RBFs

The demonstration focuses on a triangular-ground-plane points-supported shell. The supports are evenly distributed on a unit circle. The design of the ground plane leads to three free edges (boundary conditions for the stress function) and three grounded points (the Dirichlet boundary conditions for the shape function.) This subsection explains how the basis function $\phi(\cdot)$ is chosen and how the calibration points are arranged.

Suggested by Csonka [1], the curvature of the stress function $\partial_{nn}F(\mathbf{x})$ is extremely large as $\mathbf{x}$ on the edges approaches to the support points. Therefore, the RBFs should allow this singularity. To achieve such goal, the basis function $\phi(\cdot)$, scale parameters ρ_i and the centers of the sources $\boldsymbol{\mu}_i$ have to be nicely arranged. The chosen basis function is

$$\phi(\|\mathbf{x} - \boldsymbol{\mu}\|; \rho) = \sqrt{\|\mathbf{x} - \boldsymbol{\mu}\|^2 + \rho^2}, \tag{9}$$

which has a cone shape but with a blunt peak controlled by the scale parameter ρ. As ρ approaches to 0, the size of the blunt peak approaches to 0 thus the curvatures at the μ approaches to infinity. Table 2 displays few basis functions with different scale parameters and their corresponding principle stresses calculated by equation (4). When there are multiple radial basis functions acting, their effects superpose each other, similar to static electric fields exerted by multiple charged objects.

Table 2 Radial basis functions with different scale parameters.

$F(\mathbf{x}) = \lambda\sqrt{\|\mathbf{x}-\mu\|^2 + \rho^2} + c_1 x_1 + c_2 x_2$, where $\mu = (0,0)$, $\lambda = c_1 = c_2 = 1$, and		
$\rho = 0.02$	$\rho = 0.1$	$\rho = 0.5$

Understanding these properties, a basis function right on each pointy support has to be arranged and assigned with relativity small scale parameter to enable the singularity. Consequently, the source points of stress function and shape function are intentionally disturbed on the support points along with other source points within and around the domain. The scale parameters are also set differently according to the location. The parameters are smaller when source points are closer to the support. The stress function and shape function can be represented by the RBFs as

$$F(\mathbf{x}) = \sum_{i=1}^{n} \lambda_{F_i} \phi_F(\|\mathbf{x}-\mu_{F_i}\|; \rho_{F_i}) + h_F(\mathbf{x}) + \varepsilon_F, \tag{10}$$

$$z(\mathbf{x}) = \sum_{i=1}^{n} \lambda_{z_i} \phi_z(\|\mathbf{x}-\mu_{z_i}\|; \rho_{z_i}) + h_z(\mathbf{x}) + \varepsilon_z, \tag{11}$$

which can also be expressed in matrix forms as

$$\mathbf{F}(\mathbf{x}) = \begin{bmatrix} \mathbf{\Phi}_F(\mathbf{x}) & \mathbf{H}_F(\mathbf{x}) \end{bmatrix} \begin{bmatrix} \boldsymbol{\lambda}_F \\ \mathbf{c}_F \end{bmatrix} + \boldsymbol{\varepsilon}_F, \tag{10a}$$

$$\mathbf{z}(\mathbf{x}) = \begin{bmatrix} \mathbf{\Phi}_z(\mathbf{x}) & \mathbf{H}_z(\mathbf{x}) \end{bmatrix} \begin{bmatrix} \boldsymbol{\lambda}_z \\ \mathbf{c}_z \end{bmatrix} + \boldsymbol{\varepsilon}_z. \tag{11a}$$

Other than source points, the calibration points are also indispensable. For the shape equation, it should meet the Pucher's equation (5a) at the calibration points in the domain $\mathbf{x}_d$ and the Dirichlet condition (8) at the support points $\mathbf{x}_s$. The overall conditions are

$$\begin{bmatrix} \mathcal{P}_z^{\mathcal{F}}\left[\Phi_z(\mathbf{x}_d)\right] & \mathcal{P}_z^{\mathcal{F}}\left[\mathbf{H}_z(\mathbf{x}_d)\right] \\ \Phi_z(\mathbf{x}_s) & \mathbf{H}_z(\mathbf{x}_s) \end{bmatrix}\begin{bmatrix} \lambda_z \\ \mathbf{c}_z \end{bmatrix} = \begin{bmatrix} -\mathbf{p}_z \\ \mathbf{0} \end{bmatrix} - \begin{bmatrix} \boldsymbol{\varepsilon}_{\mathcal{P}z} \\ \boldsymbol{\varepsilon}_z \end{bmatrix}. \tag{12}$$

For the stress function, it should meet the Pucher's equation (5b) at the domain calibration points $\mathbf{x}_d$ and the free edge condition (7) at the calibration points on the edges $\mathbf{x}_e$. Along with the extra Dirichlet conditions to allow the stress function numerically determinate, all the conditions imposing in the stress function can be summarized by

$$\begin{bmatrix} \mathcal{P}_F^{\mathcal{Z}}\left[\Phi_F(\mathbf{x}_d)\right] & \mathcal{P}_F^{\mathcal{Z}}\left[\mathbf{H}_F(\mathbf{x}_d)\right] \\ \partial_{tt}\Phi_F(\mathbf{x}_e) & \partial_{tt}\mathbf{H}_F(\mathbf{x}_e) \\ -\partial_{nt}\Phi_F(\mathbf{x}_e) & -\partial_{nt}\mathbf{H}_F(\mathbf{x}_e) \\ \Phi_F(\mathbf{x}_s) & \mathbf{H}_F(\mathbf{x}_s) \end{bmatrix}\begin{bmatrix} \lambda_F \\ \mathbf{c}_F \end{bmatrix} = \begin{bmatrix} -\mathbf{p}'_z \\ \mathbf{F}_{tt} \\ \mathbf{F}_{nt} \\ \mathbf{0} \end{bmatrix} - \begin{bmatrix} \boldsymbol{\varepsilon}_{\mathcal{P}F} \\ \boldsymbol{\varepsilon}_{Ftt} \\ \boldsymbol{\varepsilon}_{Fnt} \\ \boldsymbol{\varepsilon}_F \end{bmatrix}, \tag{13}$$

where $\mathbf{F}_{tt}$ is given by $n_1^2\int \bar{p}_1 dx_1 + n_2^2\int \bar{p}_2 dx_2$ and $\mathbf{F}_{nt}$ is $-n_1 n_2\int \bar{p}_1 dx_1 + n_1 n_2\int \bar{p}_2 dx_2$. Since the differential operators mutually depend on each other, iterations would be needed to obtain the agreement between the stress functions and shape functions. The following sub-sections with case studies show how to implement the workflow.
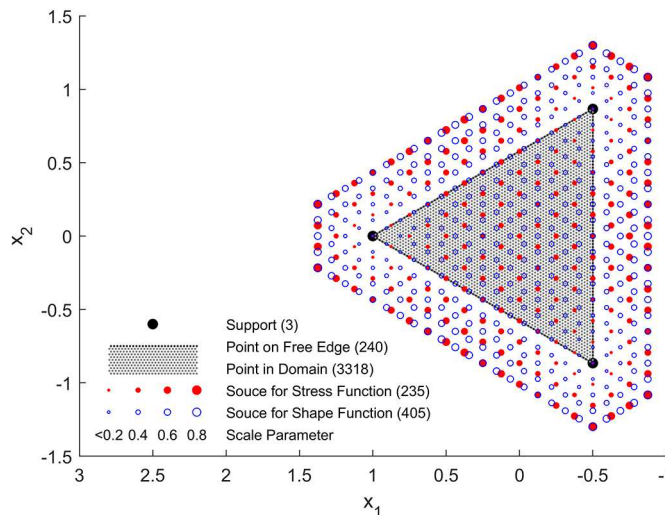

Figure 2 The distribution of all the points and their quantities (in the round brackets).

4.2. Case A: a Triangular Shell initiate from Parabola Shape Equations

The design process can either start with the stress function or the shape function. The first example shown is to initiate with a parabola shape function. By minimizing the errors in equation (13), one can derive the stress function to fit the parabola shape the most. Then, with the stress function, one can revise the shape function by minimizing the errors in equation (12). The alternating process may go forever until accuracy arrives at a certain satisfying level. The iteration process is shown in Figure 3a.

As suggested by Csonka [1], the free-edges conditions are not compatible with point-supported parabola membrane shells. As a result, the root-mean-square errors (RMSE) of the free-edge conditions initially are relatively high and drop dramatically after a few iterations while the shape has to deviate from the initial shape correspondingly. After 100 iterations, the shape function becomes another synclastic shape as shown in the first panel of Figure 4.

4.3. Case B: a Triangular Shell initiate from a Stress Function

In contrary to Case A, Case B opts to initiate the process from an analytical solution of the stress function from Csonka [1]. The initial input of the stress function goes as

$$F_{initial}(x_1, x_2) = \alpha_1 \frac{4}{3} \frac{L_0 \cdot L_1 \cdot L_2}{\alpha_2 \cdot L_0 \cdot L_1 \cdot L_2 + x_1^2 + x_2^2 - 1}, \tag{14}$$

where $L_n = \cos\left(\frac{2n\pi}{3}\right) x_1 + \sin\left(\frac{2n\pi}{3}\right) x_2 - \frac{1}{2}$, $\alpha_1 = \left.\frac{\partial F}{\partial n}\right|_{at\ L_n}$, and α_2 is a parameter influencing the peak

of the stress function ($F_{initial}(0,0) = 4\alpha_1 / 3(\alpha_2 + 8)$). In this case, α_2 is set to be 12/5 for moderate upward edges in the final shape function. The RMS of the errors in the free edge conditions (i.e. ε_{Ftt} and ε_{Fnt}) in Case B are much smaller than their counterparts in Case A. The initial stress function, which fits the boundary conditions, may contribute to the low errors in the follow-up iterations.

4.4. Case C: Triangular Membrane Shells Considering Horizontal Load

As the previous two sub-sections demonstrate, the form-finding process can either starts with shape function or stress function. In this sub-section, the horizontal loads are introduced, which are set to be constant per projected area. The process of the iteration starts with the shape function found in Case B. Then the process proceeds with alternatively minimizing the errors in equation (13) and (12) as the process described in Case A. The major difference is that $\bar{p}_2$ is set to be -0.3 instead of 0. As a result, the converged shape function has no straight edges at the boundaries as equation (7) is asking the second derivatives to follow

$$\partial_{tt} F = n_2^2 \bar{p}_2 x_2,$$
$$-\partial_{nt} F = n_1 n_2 \bar{p}_2 x_2. \tag{15}$$

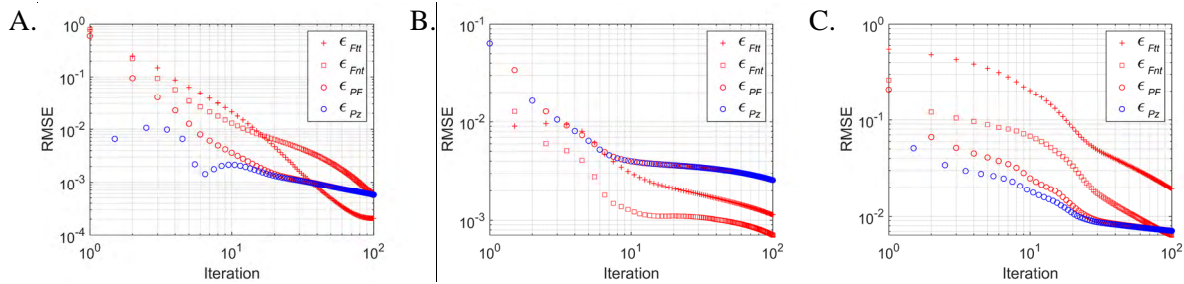The shifted stress function is shown in Figure 4.

Figure 3 The mean squared errors during the iteration process of the three cases

5. Discussions and Conclusions

This paper has proposed the workflow of applying RBFs to solve Pucher's equation and implemented it on point-supported triangular-ground-plan shells with free-edge boundary conditions. Horizontal loads have been successfully integrated. FEM modeling has confirmed that the stresses distribution has similar patterns in the prescribe one.

Arrangement of RBFs is the most critical part. The arrangement works as an implicit filter excluding all the solutions within the left null spaces. The designer should foresee the potential solutions and arrange the RBFs accordingly.

For boarder application, the follow-up works are set to be implementing the proposed method to different ground plans and boundary conditions, such as oculus and reinforced edges. Load can also be revised to none homogenously distributed.

Case A ($\bar{p}_1 = 0$, $\bar{p}_2 = 0$, $\bar{p}_z = -1$)
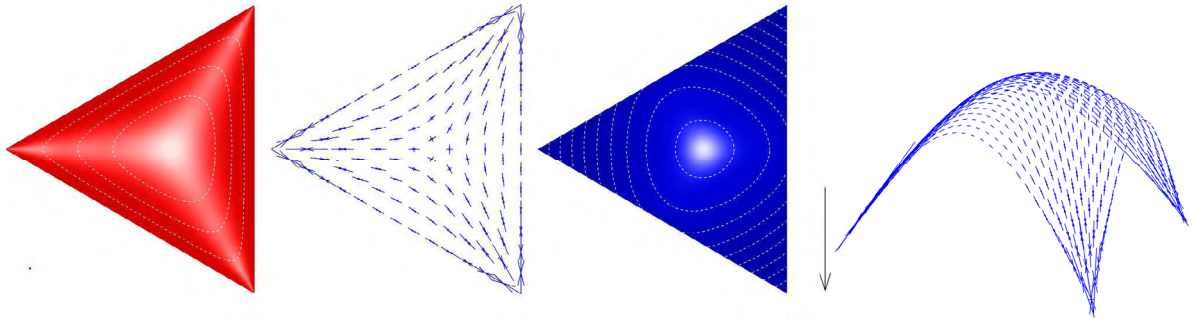
Case B ($\bar{p}_1 = 0$, $\bar{p}_2 = 0$, $\bar{p}_z = -1$)
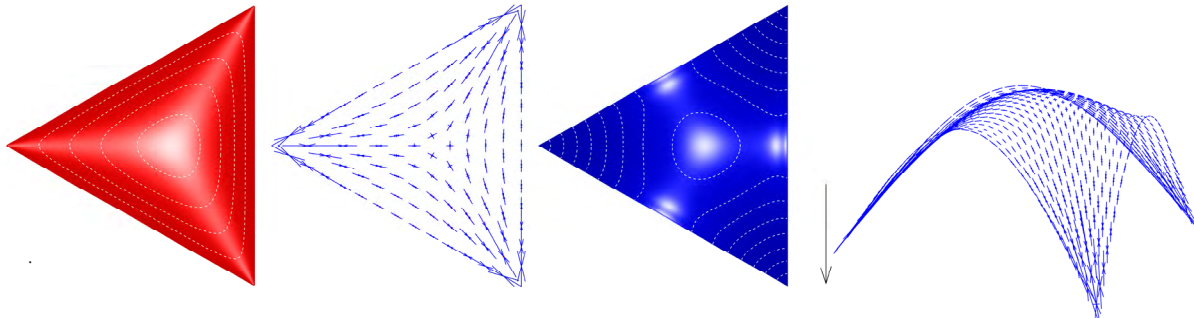
Case C1 ($\bar{p}_1 = 0$, $\bar{p}_2 = -0.3$, $\bar{p}_z = -1$)
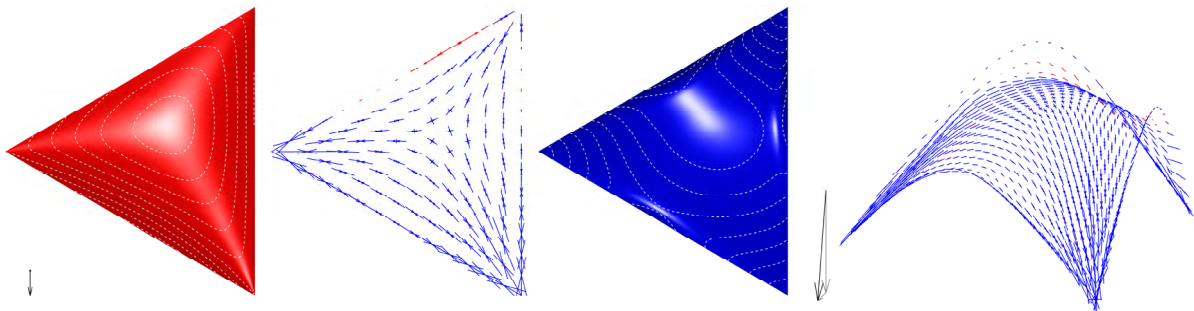

Figure 4 The converged solutions. First three columns are the top views of the stress function, stress field, shape function derived from the proposed method, and the last column is the stresses destitution calculated from FEM analysis. The back arrows suggest the directions of the loads.

References

[1]   P. Csonka, *Theory and practice of membrane shells*. VDI Verlag, 1987.

[2]   D. Veenendaal and P. Block, "An overview and comparison of structural form finding methods for general networks," *Int. J. Solids Struct.*, vol. 49, no. 26, pp. 3741–3753, 2012.

[3]   A. Pugnale, T. M. Echenagucia, and M. Sassone, "Computational morphogenesis: Design of freeform surfaces," in *Shell Structures for Architecture: Form Finding and Optimization*, S. Adriaenssens, P. Block, D. Veenendaal, and C. Williams, Eds. New York: Routledge, 2014, pp. 225–236.

[4]   M. D. Buhamann, *Radial Basis Functions*. Cambridge, 2003.

[5]   C. Chen, Y. C. Hon, and R. A. Schaback, *Scientific computing with radial basis functions*. 2005.

[6]   J. Heyman, *Equilibrium of shell structures*. Oxford: Oxford University Press, 1977.